Numerical Simulations of Rayleigh-Taylor Driven Convection in Magnetic White Dwarfs

1 Abstract

White dwarfs, representing the final stage of stellar evolution for a significant fraction of stars, are characterized by magnetic fields, the origin of which remains a subject of ongoing investigation. This study explores the hypothesis of a convective dynamo fuelled by phase separation during crystallization as a potential mechanism for the generation of these magnetic fields. The theoretical framework involves coupling the Cahn-Hilliard equation, describing phase separation phenomena, with the Navier-Stokes equations of motion, governing fluid dynamics. Computational tools like the Dedalus framework, employing spectral methods, enable the simulation of self-sustaining convective cores, offering insights into the complex processes occurring within these stellar remnants. Through three-dimensional numerical simulations, this study delves into the intricate interplay between phase separation and fluid motion within white dwarfs, providing valuable insights into their magnetic field generation.

2 Introduction

White dwarfs signify the culmination of stellar evolution and stand as one of the most prevalent endpoints for stars. It is estimated that approximately 97% of stars with initial masses ranging from 0.07 to 8 solar masses [1] conclude their evolutionary journey by transforming into white dwarfs and their evolutionary process lasts ∼10 Gyr [2]. These celestial objects are remnants of stars that have depleted their nuclear fuel and shed their outer layers. As these stars exhaust their energy sources, they undergo gravitational collapse, resulting in a dense core composed primarily of carbon and oxygen. This transformation marks the transition from a main sequence star to a white dwarf, representing the final stage in the life cycle of many stars. These objects have high densities, and there is evidence that shows a significant number of white dwarfs produce strong magnetic fields in their interiors [1]. White dwarfs have a degenerate core, where the electrons have been compressed to such high densities that they behave like a Fermi gas. This results in a range of unusual properties, such as the fact that white dwarfs do not have a well-defined surface unlike other astral objects and that their cooling properties are affected by the presence of crystallized ions in their interiors.

White dwarfs' lengthy evolution allows information to be obtained about the age of the galaxy in which the white dwarf is in and the stellar formation of the surrounding solar environment [3]. Their cores are mainly composed of carbon and oxygen, ones with lower masses tend to be made of helium and higher mass of oxygen and neon. White dwarfs tend to be highly dense $\sim 10^7$ g/cm^3 in their cores [4]. The age at which crystallization starts depends on its mass but tends to occur earlier in higher-mass stars [5]. This leads to a convective envelope forming [6]. The unique and elusive properties of white dwarfs have spurred extensive research, particularly in understanding their magnetic fields. Little is known about the precise origin of these magnetic fields; however, there are some guesses to the mechanisms that give rise to them [1]. Evidence observes that white dwarfs can generate magnetic fields spanning a wide range, from 10^3 G to 10^9 G.

There are three main theories for the origin of these magnetic fields. Progenitors of magnetic white dwarfs potentially originating from main sequence Ap/Bp stars [7] or undergoing field amplification during the helium burning phase [8]. Magnetic white dwarfs are produced by the evolution of binary systems, such as a magnetic field being amplified by a dynamo during the envelope phase [9]. Magnetic fields are generated through internal dynamo processes, similar to those observed in celestial bodies like the Earth and the Sun [10]. This dynamo process is the focus of this paper.

In a study by Isern et al. (2017), it was proposed that a core crystallization-driven dynamo might have the capability to generate magnetic fields reaching strengths of up to 10^5 G [11]. As the white dwarf cools, its inner region initiates crystallization, enriched with oxygen in its crystal phase. As

these oxygen-rich crystals grow, they descend into the inner star, augmenting the growing core while leaving behind a less dense carbon-rich fluid. This density contrast induces Rayleigh Taylor instability at the interface of the carbon-rich and the carbon and oxygen mixed fluid causing the less dense carbon fluid to rise due to buoyancy, while the denser, heavier oxygen descends, creating convection. This convective motion could potentially generate a magnetic dynamo akin to Earth's geodynamo [12], sustaining itself for gigayears. However, within the scientific community, there is ongoing debate regarding how to accurately simulate this self-consistent motion without resorting to unrealistic forcing functions to induce convection.

In this study, a self-consistent numerical model for compositionally driven convection is introduced, employing the phase-field method. The phase-field method is a mathematical framework designed to address free-boundary problems present in a wide range of physical phenomena, including crystallization and phase separation. Unlike traditional methods that require explicit boundary tracking, the phase-field approach enables the modelling of diverse microstructures with greater ease and efficiency. In this method, boundaries between different phases are represented as continuous fields that evolve dynamically as the system progresses over time. This allows for the seamless simulation of complex processes such as phase transitions and pattern formation. For this model, the phase-field method is coupled with the anelastic Navier-Stokes equations, which govern fluid motion. By integrating these two mathematical frameworks, we developed a comprehensive model capable of capturing the intricate interplay between phase separation and fluid dynamics. Specifically, the anelastic Navier-Stokes equations describe the motion of the fluid, while the Cahn-Hilliard equation characterizes the phase separation process. This coupling enables us to simulate a wide range of phenomena, such as the evolution of complex fluid flows.

3 Mathematical Theory

3.1 The Cahn-Hillard equation

The Cahn-Hilliard equation is a fourth-order partial differential equation which stands as a fundamental mathematical tool for understanding the spontaneous separation of initially uniform fluids into distinct pure phases, a phenomenon termed spinodal decomposition [13]. This process causes a homogenous binary mixture to split into separate phases with different chemical structures. It is expressed as:

$$\frac{\partial \phi}{\partial t} = M\nabla^2 \left(\frac{\partial \phi}{\partial f} - \gamma^2 \nabla^2 \phi \right) \tag{1}$$

Here, $\phi(r,t)$ represents the order parameter within the phase-field method [14], evolving over both space and time to describe the microstructure's state. The collective distribution of ϕ values constitutes the system's phase field. In the context of the Cahn-Hilliard equation, ϕ reflects the chemical composition of the system, confined within the range $-1 \leq \phi \leq 1$ [15]. Values of $\phi = -1$ and $\phi = 1$ correspond to pure component domains, while $\phi = 0$ indicates a fully intermixed homogeneous region. The parameter M denotes local mass diffusivity between the fluid components. The expression $\frac{\partial \phi}{\partial f} - \gamma^2 \nabla^2 \phi$ represents the chemical potential, encapsulating the system's energy variation as its chemical composition evolves. This energy depends on the free energy of mixing [16], $f(\phi)$, governing phase separation, and the interfacial energy term $\gamma^2 \nabla^2 \phi$, influenced solely by the compositional gradient and the interface thickness parameter γ [17]. In this context, the chemical potential can be modelled as $\phi^3 - \phi - \gamma^2 \nabla^2 \phi$, with a constant assumed for mobility.

3.2 The Cahn-Hilliard-Navier-Stokes Equations

To circumvent the numerical challenges associated with sound wave propagation, the anelastic approximation was used to model a semi-incompressible fluid with a non-constant background density profile. This choice, a common practice, proves particularly effective in contexts where sound waves play negligible roles. The anelastic approximation models fluid behaviour under semi-compressible conditions and offers a simplified representation of the compressible Navier-Stokes equations [18],

particularly suited for capturing the influence of perturbations on the background state of fluid systems. Widely applicable across shallow and deep fluid motions, it proves invaluable in modelling buoyancy-driven phenomena. By permitting variations in the fluid's background density with depth while avoiding the presence of sound waves. Under the assumption of hydrostatic equilibrium in the background state, the anelastic Navier-Stokes equations governing continuity and momentum conservation are expressed as follows:

$$\nabla \cdot (\rho_0 u) = 0 \tag{2}$$

$$\frac{\partial u}{\partial t} + (u \cdot \nabla)u = \mathrm{Re}^{-1}\nabla^2 u - \nabla(\rho_0 \delta P') + (\rho_0 \delta P')(\rho_0 \nabla \rho_0) + g(\rho_0 \delta \rho)\phi + 2\mathbf{z} \times \mathbf{u} + M(\phi^3 - \phi - \ell^2 \nabla^2 \phi)\nabla\phi \tag{3}$$

$$\frac{\partial \phi}{\partial t} + (u \cdot \nabla)\phi = M\nabla^2(\phi^3 - \phi - \gamma^2 \nabla^2 \phi) \tag{4}$$

The equations are presented in a dimensionless framework, where the spatial variable r is nondimensionalized by the stellar radius, and velocity is scaled by the characteristic linear velocity $\omega(r)$, with ω representing the rotational frequency. Time is normalized by the rotational period. This process renders key constant parameters M and γ dimensionless after the nondimensionalization of the remaining variables [19]. The vertical unit vector, denoted by $\mathbf{z}$, plays a crucial role in defining the orientation within the system. Consequently, the kinematic viscosity becomes inversely proportional to the Reynolds number (Re).

4 Simulation Framework

4.1 Dedalus Framework

The simulations were created in the Dedalus framework. Dedalus is utilized predominantly for tackling partial differential equations (PDEs), particularly in computational fluid dynamics (CFD) applications. It uses spectral methods by representing solutions through a shortened series of basis functions within a grid-based spatial domain [20]. For these simulations, a grid domain of $64 \times 48 \times 32$ points in n, ϕ, and r respectively was employed. It employs the Second-Order Backward Differentiation Formula (SBDF2) method to proficiently tackle time-dependent partial differential equations. The SBDF2 timestepper functions by breaking down the time domain into small time steps and iteratively computing the solution at each time point based on the current solution and derivative information. By leveraging the SBDF2 integrator within the Dedalus framework, a robust foundation was established for the simulations, allowing for in-depth exploration of the intricate processes occurring in stellar interiors.

The CHNS equations were solved in three dimensions within a sphere with relative radius $R = 1$, representing the radius of any white dwarf profile applied to the system. Each phase of the system is represented as $\phi = 0$, $\phi = -1$, and $\phi = 1$ which show a carbon-oxygen homogeneous fluid, pure oxygen, and pure carbon respectively.

4.2 Simulation Setup

In the initial simulation, the CHNS equations were handled independently, omitting factors such as buoyancy, surface tension, and advection. This approach aimed solely to illustrate the process of phase separation within a motionless fluid. Achieving an accurate depiction of phase separation dynamics required careful consideration of parameters like mobility and interface thickness. Determining suitable values for these parameters can be challenging due to their typically minuscule magnitudes, making them difficult to resolve numerically. To circumvent this issue in the preliminary simulations, mobility and interface thickness were treated as effective parameters, set at 10^{-5} and 10^{-9} respectively to ensure computational feasibility. The final simulation employed the fully coupled CHNS equations to emulate a self-consistent convective motion. This configuration reinstated the advection and buoyancy terms, alongside the given numerical value to the parameter $\frac{\rho'}{\rho_0}$ denoting the density change between phases of 10^{-3}, as suggested by Isern et al [1].

Phase separation was confined to a specific area within the sphere, and the simulation commenced with the introduction of small random noise perturbations to the initially uniform background profile of ϕ. In the phase field, this random noise accounts for minor deviations from the ideal phase distribution, reflecting the inherent fluctuations in the phase separation process. Similarly, in the velocity field, the noise introduces small perturbations in velocity at each point in space of the fluid. These perturbations initiate fluid motion within the simulation, thereby instigating the onset of phase separation. This approach enhances the realism of the simulation by capturing the stochastic nature of physical processes and allowing for the exploration of their impact on system behaviour.

A Gaussian density profile was selected to depict density distribution in the fluid due to its smooth, continuous nature, mirroring the expected gradient within white dwarfs peaking at the core and tapering towards the surface. A polytropic gravity function akin to an $n = 1.5$ polytrope was employed to characterize gravitational effects within the system. To minimize the viscosity and maintain stable fluid flow, a value of $\mathrm{Re} = 10^{7/2}$ was chosen.

Boundary conditions are crucial for regulating material flow and defining operational limits in the CHNS equation simulation. They eliminate shear stress and slip, stabilize fluid motion, impose zero velocity at the white dwarf's radius to confine fluid within it, fix the phase of the fluid at the boundary with a Dirichlet condition, and act as a pressure limit to maintain numerical stability.

5 Results and Discussion

5.1 Decoupled Simulation

The initial phase of our investigation involved simulating the decoupled Navier-Stokes Cahn-Hilliard equation to assess whether the Cahn-Hilliard equation accurately simulated phase separation as anticipated. A three-dimensional spherical plot was utilized to visualize the phase distribution of the fluids, ranging from approximately -1 to 1. Here, -1 represented the pure oxygen phase, 0 denoted the homogeneous carbon-oxygen phase, and 1 indicated pure carbon. Given that the uncoupled equation of motion lacked buoyancy or advection, fluid movement solely stemmed from phase separation. Consequently, the carbon-oxygen phase remained predominantly in the outer layers, while phase separation primarily occurred in the inner region, as evident in the 100th timestep frame of Figure 1. Subsequently, as the simulation progressed, the effects of the Cahn-Hilliard equation became apparent, leading to the emergence of distinct phases. Owing to the small interface thickness, the simulation plots depicted direct colour differences between the phases. In the 2000th timestep frame of Figure 1, the phase separation induced some motion, with different phases no longer confined solely to the inner region, resulting in leakage to the outer region. The 6000th timestep frame mirrored the 2000th, indicating stabilization of the simulation once phase separation was complete and no other motion factors influenced fluid movement. This simulation underscores the effectiveness of the Cahn-Hilliard equation in inducing the desired phase separation within the specified region. It demonstrates the success of our implementation of the Cahn-Hilliard equation into a multi-phase fluid system within a rotating frame of reference.

5.2 Coupled Canh-Hilliard-Navier-Stokes Simulation

Once the Cahn-Hilliard equation was confirmed to be functioning as expected, the fully coupled simulation was reintroduced by coupling it with the Navier-Stokes equations and reintegrating the buoyancy and advection terms. With motion present in this system, both velocity and phase were plotted to observe changes in motion alongside phase separation. Velocity variations are represented by colours: blue indicating motion towards the centre, red towards the boundary, and yellow signifying no motion. Initially, the simulation depicts phase separation predominantly occurring in the inner regions, leaving the oxygen-carbon phase in the outer regions. In the first frame, random fluid movement is observed throughout the system, with a faint circle around the inner region where phase separation is commencing. Next, the simulation progresses to complete phase separation in the central region, evident by distinct red and blue phase regions in Figure 2. Subsequently, in the

third frame, phase separation begins dispersing, potentially due to convection. More oxygen (blue) appears as carbon (red) disperses away from the central region, coinciding with fluid from the outer regions flowing inward, as indicated by large blue areas in the velocity plot. The final frames illustrate the inner region of the star as predominantly oxygen, with a few carbon phases dispersing outward to the edge of the simulation. The final velocity plot shows a distribution of different velocity directions, possibly indicating generalized fluid motion or minor convection.

The fully coupled simulation does not exhibit self-consistent convective motion, as the buoyancy solely induces fluid flow through density perturbations, as observed in the three-dimensional velocity plots. However, there is a distinct pure oxygen region at the centre, potentially representing the formation of a growing crystalline oxygen core typical of white dwarfs. While the model demonstrates the feasibility of a self-consistent convective system and showcases the development of an oxygen crystal core, further refinement is necessary. Specifically, the chosen values for the interface thickness require rationalization and a physical interpretation to better understand their implications within the simulation.

6 Conclusion

This study delves into the intricate dynamics of white dwarfs, focusing on the interplay between phase separation, fluid motion, and the generation of magnetic fields. Through the utilization of a self-consistent numerical model coupling the Cahn-Hilliard equation with the anelastic Navier-Stokes equations, the simulation unravelled the complex processes within these stellar remnants. Initially, by decoupling the Navier-Stokes and Cahn-Hilliard equations, the progression of phase separation solely influenced by compositional gradients was observed. Visualization of the phase distribution confirmed the efficacy of the Cahn-Hilliard equation in inducing phase separation within the designated region. Subsequent reintroduction of the fully coupled simulation, incorporating buoyancy and advection terms, allowed for the observation of the interplay between fluid motion and phase separation. Although the simulation did not exhibit self-consistent convective motion, it revealed intriguing patterns suggestive of the formation of oxygen-rich cores characteristic of white dwarfs. The findings underscore the potential of compositionally driven convection to sustain magnetic dynamo processes within white dwarfs, shedding light on the origins of their magnetic fields.

7 Future Work

Should the buoyancy function be modifiable to ensure self-consistent convection, it becomes feasible to compute the kinetic energy associated with fluid motion. This, in turn, facilitates the determination of the potential magnetic field generated by ions within the core of a white dwarf during convection. Such analysis aids in assessing the viability of the dynamo theory in explaining the origin of magnetic white dwarfs.

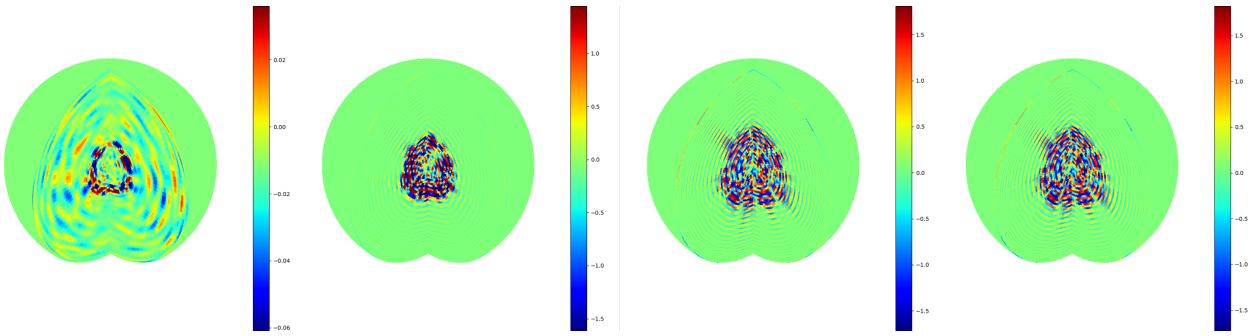

Figure 1: 3D phase plot at time step: 100, 400, 2000, 6000

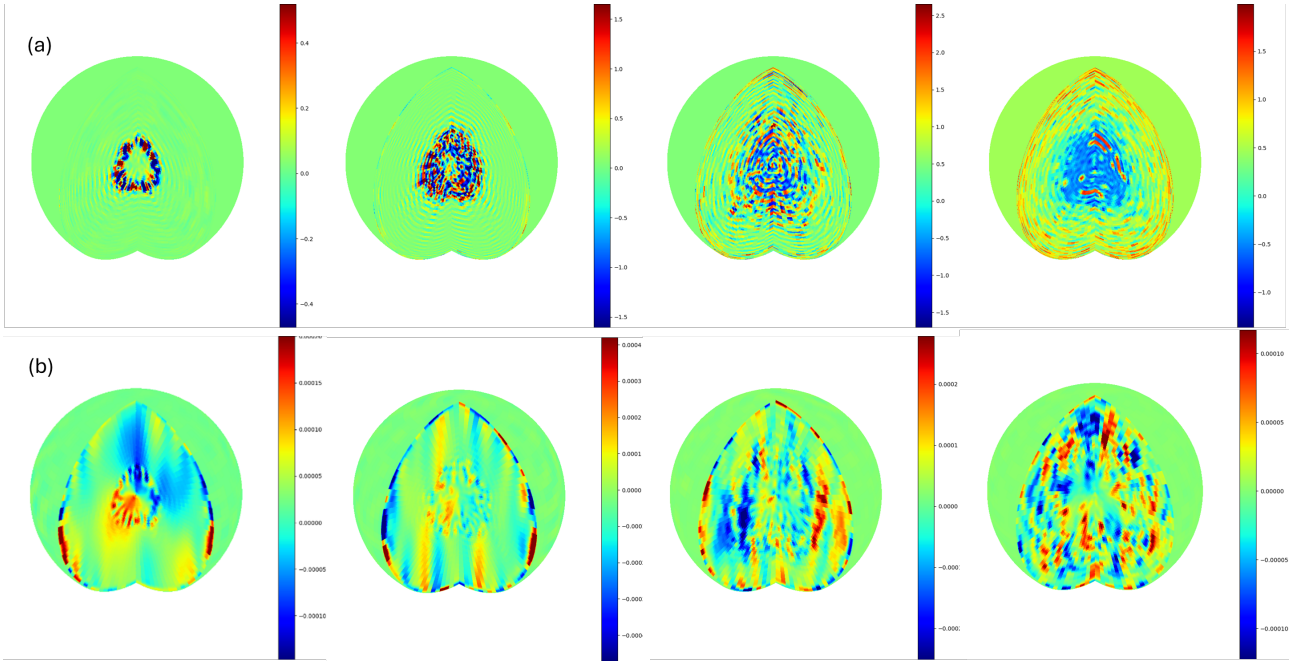

Figure 2: 3D phase plot(a) and corresponding velocity plot(b) at time step: 200, 1000, 3000, 10000

References

[1] Angel, J.R.P., Borra, E.F., & Landstreet, J.D. (1981). The magnetic fields of white dwarfs. *Astrophysical Journal Supplement Series*, *45*, 457-474.

[2] van Horn, H.M. (1968). Crystallization of White Dwarfs. *The Astrophysical Journal*, *151*, 227. Available at: `https://ui.adsabs.harvard.edu/abs/1968ApJ...151..227V/abstract`.

[3] Fauve, S., & Petrelis, F. (2003). The dynamo effect. *Peyresq lectures on Nonlinear phenomena*, 2, 1-64.

[4] Ferrario, L., de Martino, D., & Gänsicke, B.T. (2015). Magnetic White Dwarfs. *Space Science Reviews*, *191*(1-4), 111–169.

[5] Fontaine, G., Brassard, P., & Bergeron, P. (2001). The Potential of White Dwarf Cosmochronology. *Publications of the Astronomical Society of the Pacific*, *113*(782), 409–435.

[6] García-Berro, E., Lorén-Aguilar, P., Aznar-Siguán, G., Torres, S., Camacho, J., Althaus, L.G., Córsico, A.H., Külebi, B., & Isern, J. (2012). Double degenerate mergers as progenitors of high-field magnetic white dwarfs. *The Astrophysical Journal*, *749*(1), 25.

[7] García-Berro, E., Torres, S., Althaus, L.G., Renedo, I., Lorén-Aguilar, P., Córsico, A.H., Rohrmann, R.D., Salaris, M., & Isern, J. (2010). A white dwarf cooling age of 8 Gyr for NGC 6791 from physical separation processes. *Nature*, *465*(7295), 194-196.

[8] Isern, J., & Garcia-Berro, E. (n.d.). WHITE DWARFS AND THE AGE OF THE UNIVERSE. Available at: `https://www.slac.stanford.edu/econf/C0307073/papers/JI.pdf`.

[9] Isern, J., García-Berro, E., Hemanz, M., & Mochkovitch, R. (2002). Crystallizing White Dwarfs. *Strongly Coupled Coulomb Systems*, 251–254.

[10] Levy, E.H., & Rose, W.K. (1974). Production of magnetic fields in the interiors of stars and several effects on stellar evolution. *The Astrophysical Journal*, *193*, 419-427.

[11] Isern, J., García-Berro, E., Külebi, B., & Lorén-Aguilar, P. (2017). A common origin of magnetism from planets to white dwarfs. *The Astrophysical Journal Letters*, *836*(2), L28.

[12] Lister, J.R. (1994). How much of the Earth's core would be stably stratified if Nu ¡ 1?. In *Proceedings of the 4th SEDI Symposium on Earth's Deep Interior*. Whistler Mountain, British Columbia, Canada.

[13] Wodo, O., & Ganapathysubramanian, B. (2011). Computationally efficient solution to the Cahn–Hilliard equation: Adaptive implicit time schemes, mesh sensitivity analysis and the 3D isoperimetric problem. *Journal of Computational Physics*, *230*(15), 6037-6060.

[14] Li, J., Zheng, D., & Zhang, W. (2023). Advances of Phase-Field Model in the Numerical Simulation of Multiphase Flows: A Review. *Atmosphere*, *14*(8), 1311.

[15] Novick-Cohen, A. (2008). The cahn–hilliard equation. In *Handbook of differential equations: evolutionary equations*, 4, 201-228.

[16] Cahn, J.W., & Hilliard, J.E. (1958). Free energy of a nonuniform system. I. Interfacial free energy. *The Journal of Chemical Physics*, *28*(2), 258-267.

[17] Magaletti, F., Picano, F., Chinappi, M., Marino, L., & Casciola, C.M. (2013). The sharp-interface limit of the Cahn–Hilliard/Navier–Stokes model for binary fluids. *Journal of Fluid Mechanics*, *714*, 95-126.

[18] Kupka, F., & Muthsam, H.J. (2017). Modelling of stellar convection. *Living Reviews in Computational Astrophysics*, *3*, 1-159.

[19] Conesa, M., Sánchez Pérez, J.F., Alhama, I., & Alhama, F. (2016). On the nondimensionalization of coupled, nonlinear ordinary differential equations. *Nonlinear Dynamics*, *84*, 91-105.

[20] Burns, K.J., Vasil, G.M., Oishi, J.S., Lecoanet, D., & Brown, B.P. (2020). Dedalus: A flexible framework for numerical simulations with spectral methods. *Physical Review Research*, *2*(2), 023068.